Increasing wind farm efficiency by yaw control: beyond ideal studies towards a realistic assessment

Increasing wind farm efficiency by yaw control: beyond ideal studies towards a realistic assessment

U Ciri, M A Rotea and S Leonardi

The UTD Center for Wind Energy
Department of Mechanical Engineering, The University of Texas at Dallas, Richardson TX 75080, USA

E-mail: stefano.leonardi@utdallas.edu

Abstract. Recent studies have demonstrated promising results for yaw control to mitigate wake interactions and optimize wind farm efficiency. These studies have been carried out for a single 'ideal' operating condition, typically assuming a fixed wind direction and speed. In a real scenario, the wind speed and direction change continuously over time, including cases in which yaw control does not provide any improvement. Thus, results from idealized studies cannot be generalized to estimate annual energy production (AEP) improvements in real scenarios with sufficient accuracy. In this paper, we provide a method to estimate the impact of yaw control on annual energy production, based on high-fidelity simulations. The stochastic procedure leverages high-fidelity numerical simulations to obtain a surrogate model with generalized Polynomial Chaos (gPC). For a single wind direction improvements of the order $\sim 10\%$ are obtained; which is typical of an ideal estimate. On the other hand, the AEP gain is about 3% for the entire wind farm under realistic variable wind directions. The magnitude of the AEP gain is site-dependent. The proposed methodology provides an accurate tool useful for evaluating the value proposition of yaw control for wake steering.

1. Introduction

Recent studies have demonstrated promising results for control strategies such as yaw control to mitigate wake interactions and optimize wind farm efficiency [1–5]. In general, these studies have been carried out for a single 'ideal' operating condition, typically assuming a fixed wind direction and speed. However, wind farm performance is usually measured considering metrics such as annual energy production (AEP), which entails operations over a wide range of wind conditions. Wind conditions at a wind farm site include cases in which there is little to no value added for optimization. For instance, depending on the layout, no wake interactions may occur for certain wind directions, or the wind speed may be above-rated value and power production already maximized at nominal capacity. Hence, the efficiency improvement in a real wind farm will likely be lower than the power gains predicted by idealised studies when measured in terms of AEP.

AEP is a key metric because it directly affects the levelized cost of energy and hence plant revenue. Therefore, the implementation of a novel control strategy, such as yaw control, requires an accurate estimate of the impact of the control strategy on AEP. The current practice in research and industry to estimate and optimize AEP relies on wake models because of the low computational cost [6]. However, it is challenging to obtain accurate predictions for wind farm

operations with wake models. In particular, parameterization of wake deflection by yaw (which is the fundamental mechanism for yaw control) is still an open issue in wind energy research. As a result, the estimate of AEP from a wake model is inevitably affected by a possibly large uncertainty, and it may be difficult to draw conclusions on the value of optimization strategies given the limited gain margins.

Conversely, large-eddy simulations (LES) coupled with a rotor model have shown ability to accurately capture wind farm performances. Because of the computational cost, the direct evaluation of AEP with LES is not feasible yet. In this contribution, we propose a methodology to overcome these limitations and obtain an estimate of AEP, which is based on high-fidelity simulations. The goal is to achieve a realistic assessment of the benefit of yaw control on wind farm AEP.

2. Methodology

The AEP is the expected value of energy produced by the plant over the course of one year (T):

$$\mathrm{AEP} = T \cdot \int_{\Omega} P_{\mathrm{farm}}(U,\theta;q) \cdot PDF(U,\theta)\ d\Omega, \tag{1}$$

where Ω is the "event space", i.e. the combinations of wind speed U and direction θ experienced at the site, and $PDF(U,\theta)$ is the joint probability density function of wind speed and direction (i.e. the wind rose at the site). $P_{\mathrm{farm}}(U,\theta;q)$ is the power produced by the wind farm. The power is a function of the wind conditions and the control parameters, synthetically indicated in (1) with q.

A stochastic methodology is employed for estimating the integral in equation (1):

(*i*) sample the probability distribution of the uncertain independent variables (U and θ);

(*ii*) evaluate wind farm power production P_{farm} as a function of the sampled (U,θ) combinations;

(*iii*) perform a statistical analysis of the responses at step (*ii*) to obtain AEP.

In the first step, the distribution of wind speed and direction is swept with the Latin Hypercube Sampling (LHS) method [7]. LHS is a sampling technique similar to Monte Carlo (MC) methods [8]. While in MC methods samples are drawn in a random fashion, in LHS samples are selected so that each equally probable interval of the parameter range is equally sampled. This improves the convergence of the statistical output quantities, reducing the number of samples required for a given accuracy level [9]. The LHS samples are then used to obtain the system response at step (*ii*), that is the value of power produced for the input wind speed and direction. This is accomplished through the use of a surrogate model for the wind farm power production, which is the core of the method. The responses are processed to calculate the statistical properties of the power production, including the estimate of AEP, equation (1).

To evaluate the impact on AEP of an optimized yaw control strategy 'q_{opt}', two surrogate models are built: one for the baseline control strategy $P_{\mathrm{base}} = P_{\mathrm{farm}}(U,\theta;q_{\mathrm{base}})$; and one for the optimized case, $P_{\mathrm{opt}} = P_{\mathrm{farm}}(U,\theta;q_{\mathrm{opt}})$. Following the stochastic procedure, AEP is computed for both surrogate models and the estimate of the potential AEP gain is obtained.

The surrogate model is derived combining generalized polynomial chaos expansion and high-fidelity simulations. Generalized Polynomial Chaos (gPC) expansion is a technique to describe the evolution of a random process depending on uncertain input parameters [10, 11]. With this approach, the wind farm power production is treated as the "random process" function of the naturally uncertain input variables U and θ. The gPC expansion, truncated at order N, of the farm power production is given by:

$$P_{\mathrm{farm}}\left(U,\theta;q\right) = \sum_{j=1}^{N} \alpha_j \varphi_j(U,\theta)\,, \tag{2}$$

where φ_j are orthogonal polynomials, which depend on the probability density function of the input parameters (U, θ). The polynomial basis is optimal in the sense that the truncated expansion (2) has the fastest convergence to the functional P_{farm} [10–13]. Therefore, a relatively low order of expansion provides an accurate representation of P_{farm}.

The order of the truncation, N, depends on the number of uncertain variables, n, and the order of the polynomial of highest degree, p_i, selected for each uncertain variable:

$$N = \prod_{i=1}^{n} (p_i + 1) \,. \tag{3}$$

The coefficients α_j are obtained as the Galerkin projection of the response function over the element of the basis φ_j:

$$\alpha_j = \frac{\langle P_{\text{farm}}, \varphi_j \rangle}{\langle \varphi_j, \varphi_j \rangle}, \tag{4}$$

where $\langle \cdot, \cdot \rangle$ indicates the generalized scalar product in the event space under which the basis polynomials are orthogonal:

$$\langle f, g \rangle = \int_{\Omega} f(\xi)\, g(\xi)\, \rho(\xi)\, d\xi, \tag{5}$$

where $\rho(\xi)$ is the weight function associated with the polynomial family. The coefficients α_j are unknown a priori, but can be determined using N deterministic realizations of the random process. In the present case, these realizations consist in N high-fidelity simulations of the wind farm performed for specified combinations of U and θ. For each random variable, the input values for the simulations are taken as the roots of the $p_i + 1$ polynomial associated with the probability density function of the variable. In this way, the integrals in equation (4) can be accurately evaluated using Gaussian quadrature.

High-fidelity LES with turbine actuator model constitute the underlying flow model, which is needed to obtain accurate predictions. In a recent work [14], this procedure has been validated for a wind farm in north Texas and compared with predictions from a widely-used wake model [15,16]. The error in the estimate of the mean power compared to SCADA data is limited to 2%, which provides an improvement of over 90% respect to the wake model. Therein [14], it has been also presented an extension of the gPC procedure to obtain a control-oriented surrogate model. This is done by assuming the control strategy parameter q as an additional uncertain variable. The resulting polynomial expansion can then be maximized respect to the control parameter(s) with a classic optimization algorithm (e.g. a gradient-based method as done, for example, in [14]). We note that using such an expansion the gPC procedure could provide the optimal yaw angles as a function of the wind conditions. In this paper, the optimal yaw angles will be determined for the expansion points only as described in Section 3.2. This will provide the representative improvements of the optimized control strategy and will permit to evaluate the overall impact of yaw control on AEP.

3. Test case

We have applied the procedure described in Section 2 to a wind farm in Europe. Figure 1*a* shows the layout of the farm and contours of the local topographic elevation. The farm consists of 9 wind turbines, which are deployed on a slope. All the turbines are identical, with rotor diameter $D = 52$ m and rated power $P_{\text{rated}} = 850$ kW. Measurements from the supervisory control and data acquisition (SCADA) system were available for this wind farm. Unfortunately, it was not possible to access additional meteorological data (e.g. from a nearby met mast) for this site to obtain direct knowledge of the free-stream wind conditions (necessary for the procedure). Therefore, a synergistic analysis of SCADA data and LES has been conducted to infer the free-stream conditions from the measurements at the turbines. The site wind rose extrapolated from

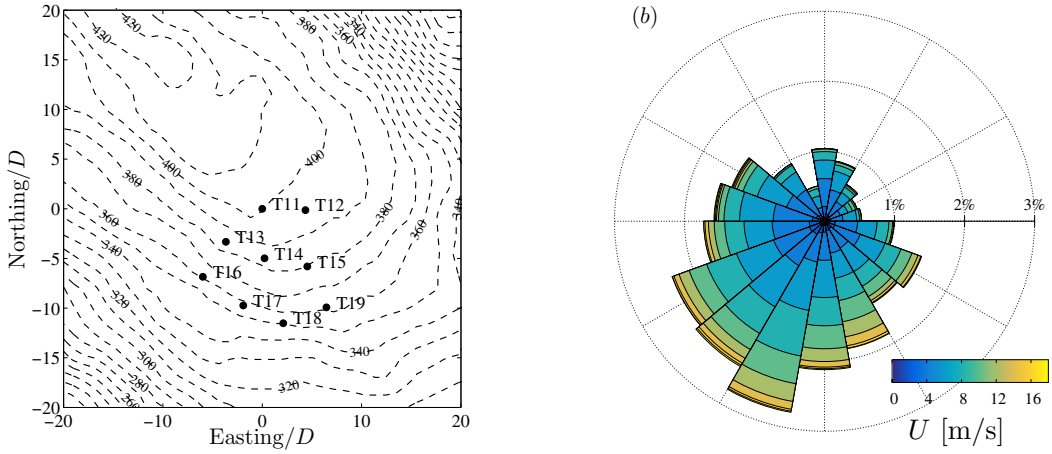

Figure 1. Test case wind farm: (a) turbine layout with superimposed topography iso-levels. Contours levels from 200 m.a.s.l to 450 m.a.s.l. every 10 m; (b) wind rose at the site, extrapolated from available SCADA data.

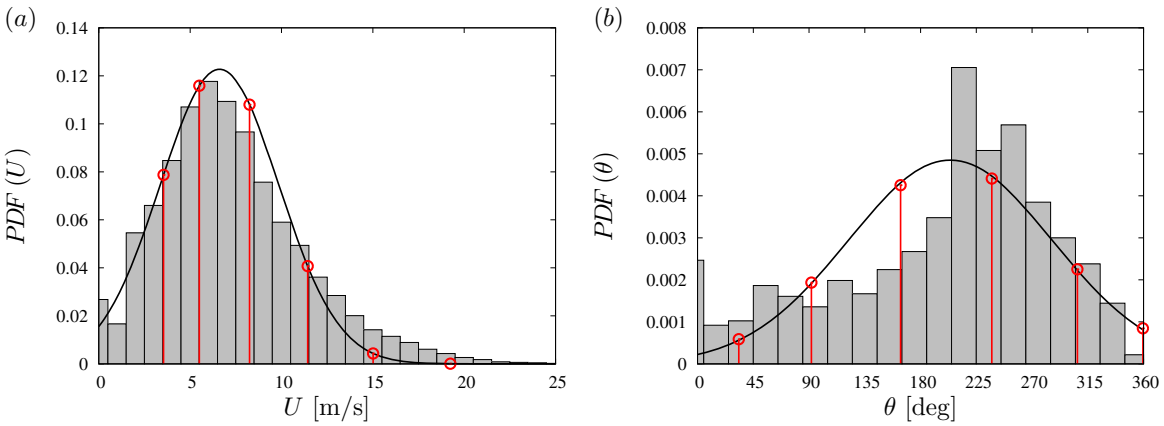

Figure 2. Probability density function of wind speed (a) and wind direction (b): ■ SCADA data; ○ expansion points; —— normal distribution fit: (a) mean value $\mu = 6.6$ m/s and standard deviation $\sigma = 3.25$ m/s; (b) $\mu = 200°$ and $\sigma = 85°$.

SCADA data is shown in Figure 1b. The wind is predominantly from the South-West sector, although overall the variability is quite large. The distribution is qualitatively corroborated from low-altitude wind data gathered from nearby airport stations (not shown here).

Figure 2 shows the PDFs of the wind speed and direction obtained from the wind rose in Figure 1b. The figure compares the raw data from SCADA with a numerical fit using normal distributions. A normal distribution fits the data from SCADA to a good approximation. As a consequence, Hermite polynomials are selected as the optimal basis for the gPC expansion. The expansion is truncated to the 5^{th} degree for both variables ($p = 5$), which results, according to equation (3), into $N = 36$ terms. For each variable (wind speed and direction), the sampling points of the gPC expansion are determined by the roots of the (univariate) polynomial of degree $p + 1$. Figure 2 shows the sampling points for wind speed (a) and direction (b). The $N = 36$ deterministic realizations are obtained by tensorially combining each value of U and θ. The wind direction expansion points span quite evenly the compass horizon, with two northerly wind directions (the first and last points, $\theta = 30°$ and $355°$), one southern direction ($\theta = 160°$),

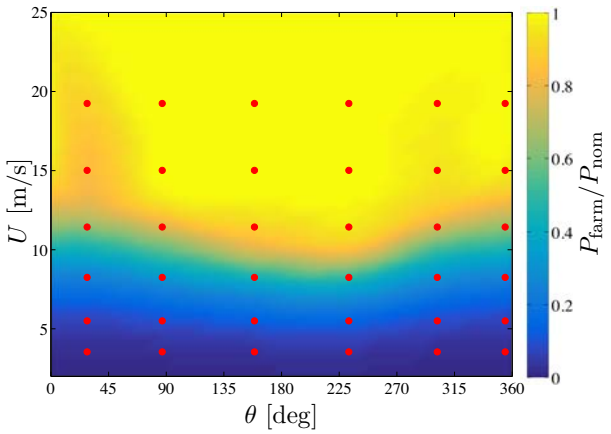

Figure 3. Wind farm power production, normalized by the nominal plant capacity P_{nom}, as a function of wind speed and direction computed with the gPC expansion. The red dots indicate the sample points.

two cases with wind from the West and East, respectively, and a latter case at $\theta \sim 230°$, which is close to the predominant wind direction. For the wind speed, the sampling points include four values in the turbine Region II envelope ($U < 13$ m/s, which is the rated value), and two cases in Region III (above rated).

For each expansion point, numerical simulations are performed using our in-house code [17, 18]. The Smagorinsky model [19] with constant $C_s = 0.11$ is used for the subgrid stresses in the large-eddy simulations. The turbine blades are represented with the rotating actuator disk model [20], while tower and nacelle are directly included in the simulations with the immersed boundary method [21]. The immersed boundary method is also used for the local topography (Figure 1a). For every expansion point, the computational domain is rotated to have a coordinate axis in the direction of the flow. The wind farm is centered in the middle of the domain, which is $25.2D$ long in both the spanwise and streamwise directions. To minimize the blockage effect due to the presence of the topography, the domain range in the direction normal to the ground is increased to $20D$. In the domain region around the wind turbines, the grid resolution is uniform and equal to $\delta/D = 0.035$ in all the directions. Realistic inflow conditions with shear and turbulence are obtained from a precursor simulation over a flat terrain with roughness cubes of size $0.2D$ on the ground [22].

3.1. Baseline surrogate model

For each sample identified with the gPC procedure, a first simulation is performed for the baseline control strategy. That is, turbines are operated with a standard two-region control scheme [23, 24] and without yaw control for wake steering. For the Region II wind speeds, the numerical simulations have been performed for the six wind directions at one nominal value of wind velocity ($U = 8.3$ m/s). Data for the other velocity points have been computed using dynamic similarity (all the relevant non-dimensional numbers in the governing equations are virtually the same). On the other hand, because of possible wake interactions, it is not possible to establish a priori any dynamic similarity between the last two velocity points ($U = 15$ and 19.2 m/s), and the simulations have been carried out for both cases.

Using the results from all the sample points, the expansion coefficients α_j can be determined with equation (4). Figure 3 shows the resulting surrogate model, that is the farm power production as a function of wind direction and speed. As expected, the power production increases with the wind speed and saturates to the nominal capacity ($P_{\mathrm{nom}} = 9 \cdot P_{\mathrm{rated}}$, as the

farm consists of 9 turbines) for $U > V_{\text{rated}} = 13$ m/s. The map also shows that northerly wind directions tend to yield less power production. Flow visualizations (not shown here) confirm that these cases suffer by a significant amount of wake interactions. However, according to the wind rose in Figure 1*b*, these under-performing wind directions have limited probability of occurence.

The performance map in Figure 3 essentially constitutes the surrogate model which is required for the stochastic methodology to estimate AEP. The wind distribution is swept with the LHS, processed with the surrogate model and statistically analyzed. The error in the prediction of the total power compared to the SCADA measurements is 8%, and for most turbines the power is accurately predicted within the $\pm 10\%$ band. The agreement is fairly good, especially in consideration of the large uncertainties associated with the present test case (e.g. complex topography and absence of met-tower data for accurate computation of the wind distribution).

3.2. Optimization of annual energy production

A set of wind speed and direction combinations have been selected for the optimization. To minimize the computational costs associated with the optimization, we have selected three wind directions from the sample points of the gPC expansion. In principle, the optimization can be extended to all the sample points in the gPC expansion, which increases the potential for improving the plant capacity factor. The optimization has been performed for the two northerly wind directions ($\theta = 28^\circ$ and 354°), which have the lowest performance and present significant wake interactions, and for $\theta = 232^\circ$, which is also affected by wake interactions among the turbines and is a common wind direction under which the plant operates.

The optimization study is conducted by performing LES at the nominal Region II wind speed. Results are scaled for entire below-rated regime using dynamic similarity. In Region III, above rated speed, no optimization is performed, because the power is already limited at maximum capacity.

Yaw control is employed to improve power production. Herein, extremum-seeking control (ESC) is used to determine the optimal misalignment angles of the turbines. In general, for this step of the procedure one could also use a different optimization algorithm, or also select another turbine control parameter to improve power production (e.g., the torque gain). Extremum-Seeking Control is a model-free closed-loop control algorithm, which implements the gradient method for optimization without the need of a physical model of the system [25, 26]. We use ESC in the nested version (NESC) described in [27,28] for wind farm power optimization. NESC is applied to clusters of a upstream and downstream turbines coupled by wake interactions. For each cluster, the algorithm iteratively adjusts the yaw angle of the upstream turbine to the value which optimizes the following performance index:

$$J(t) = P_{\text{upstream}}\,(t - \tau) + P_{\text{downstream}}(t), \tag{6}$$

where P is the power of the individual turbines and τ is a time delay between the turbines due to wake propagation (which is required because the algorithm operates on-line [27]). At each iteration the yaw angle is changed based on the (estimated) gradient of the performance index respect to the yaw angle.

Figure 4 shows the details of the optimization procedure for the northerly wind directions (top two rows; a, b, c, d) and for $\theta = 232^\circ$ (e, f). Visual inspection of flow visualization from the baseline case is used to select the turbine clusters on which the algorithm is applied. The left-hand side figures report the value of the yaw misalignment adjusted by NESC as a function of time. The algorithm is turned on around $t = 0$, with a small shift in time among the various turbines to prevent cross-correlation. The initial yaw misalignment angle on some turbines is different from zero. This angle has been determined from a preliminary combined analysis of SCADA data and LES. Convergence is attained in about 20–30 minutes, after which the algorithm is turned off and the yaw misalignment is set to the mean value identified by the

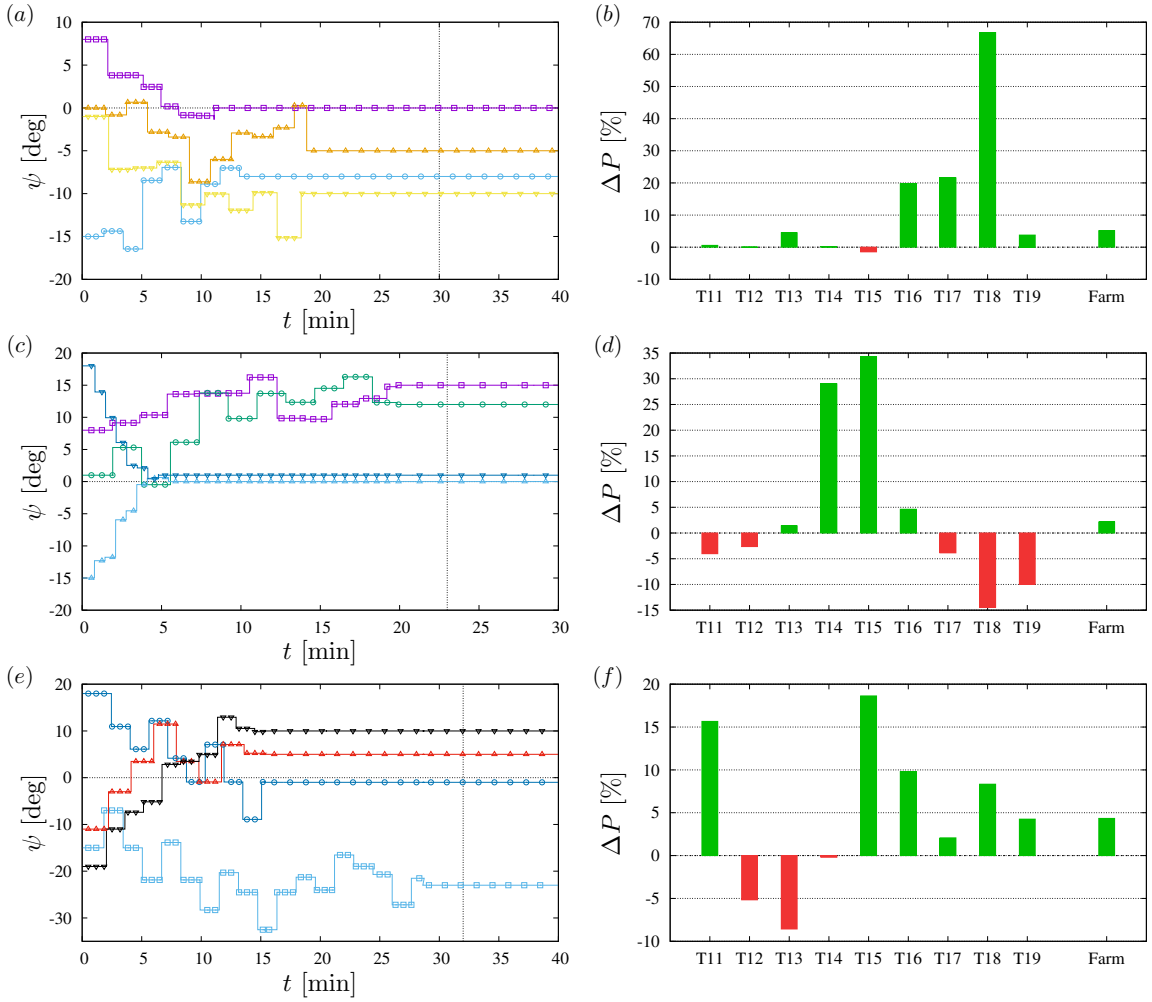

Figure 4. Optimization procedure for the selected wind directions: (a, b) $\theta = 28°$, (c, d) $\theta = 354°$, (e, f) $\theta = 232°$. Left figures, time history of yaw misalignments adjusted by NESC: (a) ■ T11, ● T13, ▲ T14, ▼ T15; (c) ■ T11, ● T12, ▲ T13, ▼ T16; (e) ■ T13, ● T16, ▲ T17, ▼ T18. Right, power improvement respect to baseline control strategy. The vertical lines in the left figures denote the time instant after which steady-state values are computed.

algorithm. The power improvement respect to the baseline strategy (shown in Figure 4b, d and f) is evaluated in this latter condition, after the transient optimization is ended. The relative gain on the individual turbines can be quite significant, similarly to the yaw control studies in ideal scenarios. The increase reaches double-digit figures, with peaks up to 30% or even 70% for the single conditions. The variation on some turbines is negative, owing to the misalignment induced by NESC.

As an example, Figure 5 compares the wind field for the wind direction $\theta = 230°$, before (a) and after (b) the optimization. The effect of the topography slope is evident from the visualizations. The terrain creates a favorable pressure gradient when the inclination is uphill, which accelerates the flow throughout the wind farm [29]. The algorithm increases the misalignment on turbine T13, which generates a large wake deflection. This is beneficial for turbine T11, which augments power production by more than 15%, compensating the decrease in power production on turbine T13 ($\sim$ 8%). At the same time, the power loss on T13 is

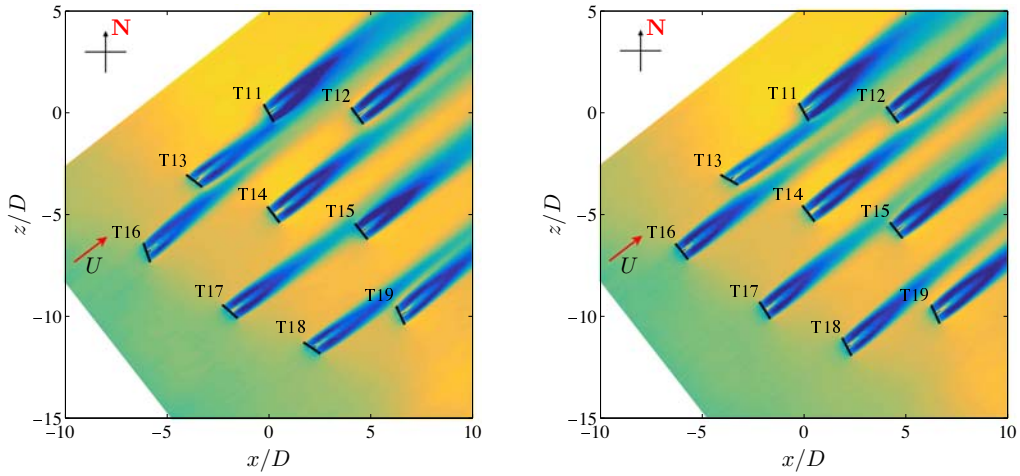

Figure 5. Visualization of the wind field at hub height for the case $\theta = 232°$: (a) baseline control strategy; (b) after NESC optimization.

mitigated by the NESC algorithm on turbine T16. In this case, NESC essentially eliminates the initial yaw misalignment, present in the baseline distribution. Thus, the power of turbine T16 increases by about 10%, and the wake is straightened and deflected away from the area swept by the blades of turbine T13. However, the wake of turbine T16 partially impinges on the turbine T12 further downstream. The streamwise separation between this two turbines is large (about $12.5D$), and the reduction on the downstream turbine is marginal (5%). Furthermore, the optimization algorithm is applied to turbine T17 and results in a change in sign in the yaw misalignment, from $-10°$ to about $5°$. As a result, the downstream turbine T15 is exposed to the free-stream wind, which yields the largest power gain of all turbines for this wind direction (almost 20%). The yaw offset of the dithering turbine, T17, reduces in magnitude and its power production increases. This is the case also for turbine T18, which is driven to narrower yaw misalignment (in absolute value) favorable for both turbines in the cluster, T18 and T19.

Similar arguments can be made for the changes observed in the other wind directions considered ($\theta = 28°$ and $354°$). In general, the optimization procedure improves performances not only through the coordinated active wake steering control, but also by mitigating the initial baseline yaw misalignment, which is not optimal for all the wind directions. Thus, a yaw-based individual extremum-seeking controller could additionally be implemented on all turbines in the plant to minimize losses due to yaw errors, thus providing a lower bound on the potential gain which can be achieved. For instance, [30] reports that operation inefficiencies, including yaw misalignment, can amount to losses up to 2% of AEP.

Overall, the improvement in the power plant power production attains lower levels, because of the balance among the variations on all the turbines. The best gain is about 5% for $\theta = 28°$ and $\theta = 232°$, while the case $\theta = 354°$ provides a lower performance gain (2.5%). Using these optimized conditions, a new surrogate model is obtained for the optimized control strategy, $P_{\text{opt}} = P_{\text{farm}}(U, \theta; q_{\text{opt}})$. Then, the surrogate model is used within the stochastic procedure (LHS) to estimate the AEP and evaluate the impact of the yaw control strategy. Figure 6 shows the percentage improvement in AEP for the entire farm and each individual turbine. The plant performance is improved by about 3%. Analogous studies on AEP optimization, albeit based on wake models, reach power improvements of similar magnitude [31–35]. The limited power gain compared to the values obtained in the previous studies and also for the individual optimization cases considered herein (Figure 4) is not surprising. As anticipated in the introduction, over the course of one year (for AEP estimation, but the same holds in general for the farm operating

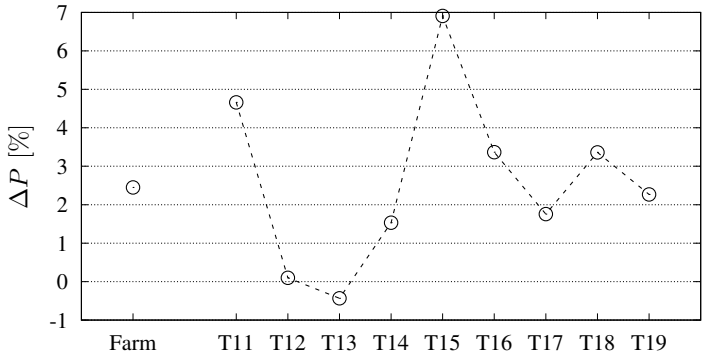

Figure 6. Percentage improvement in annual energy production yielded by yaw control over the baseline control strategy.

life), wind conditions significantly vary at the farm. This includes hours of operation for which no optimization is feasible, because, for example, the turbines are operating in Region III or no wake interactions occur. Clearly this limits the outcome of any optimization control strategy, and an improvement in AEP larger than about $3-5\%$ is probably only possible if the initial design is severely under-performing.

Although the AEP gain is lower than the baseline error with respect to SCADA data ($\sim 8\%$), it reasonably still represents a meaningful improvement. In fact, the baseline error is probably due for the most part to the uncertainty in the incoming wind conditions extrapolated from the SCADA data. When evaluating AEP, this bias on the estimate is present for both the baseline and the optimized surrogate model. Therefore, the uncertainty on the AEP gain is much lower than for the single control strategies (baseline or individual), and the gain obtained can be considered as an actual realistic improvement.

Figure 6 shows that larger power improvements can be obtained on the individual turbines. For instance, the increase in AEP for turbine T15 is about 7%, which is quite significant. Turbine T15 is deployed in the middle of the farm, For this reason, it is likely affected by wake interactions over a wide range of wind directions, and thus has a comparatively lower baseline respect to the other turbines in the farm. Therefore, in this case the optimized control strategy can be very profitable. On the other hand, it is also observed that AEP is slightly decreased for turbine T13. This is related to the fact that, in the optimized control strategy, this turbine has a large yaw misalignment, and a consequent curtailment in power compared to the baseline, for southerly winds which are the most common at the site. However, this power loss is largely compensated by the improvements induced by the yaw angle on the other turbines, and the overall effect of the optimized control strategy is beneficial for the farm.

4. Conclusions

A stochastic procedure to estimate annual energy production combining generalized Polynomial Chaos and high-fidelity simulations has been presented. The procedure has been used to evaluate the impact of power optimization through yaw control on a real wind farm, in realistic conditions. Previous yaw control studies in the literature have been performed in idealized configurations, such as a fixed wind direction. However, because of the inherent variability in an actual wind farm, these studies cannot be generalized with sufficient accuracy to estimate annual energy production improvements. In this paper, we provide for the first time a method to estimate the impact of yaw control on annual energy production, based on high-fidelity simulations.

The stochastic procedure leverages high-fidelity numerical simulations to obtain a surrogate

model with generalized Polynomial Chaos (gPC). The resulting surrogate model has a low computational cost (it is a polynomial), but maintains a high-level of accuracy because of the high-fidelity data embedded in the model and because the polynomial basis is tailored to the wind conditions at the site. The annual energy production is the computed by sweeping through the Latin Hypercube Sampling technique the wind speed and direction distributions, and using the surrogate model to obtain the farm response to each incoming wind sample.

Two surrogate models are obtained, one for the baseline control strategy and one using yaw control optimization. The nested Extremum Seeking Control algorithm is employed for the optimization. While for a single wind direction, NESC is able to yield an improvement of about $5-10\%$ for the farm power production, the improvement of AEP is about 3% for the entire wind farm. As expected, due to the variability of wind conditions in a realistic scenario, the magnitude of the energy gain is reduced compared to results obtained in idealised configurations. The optimal control strategy and its impact on annual energy production is site-dependent and has to be evaluated case by case. From a practical point of view, the estimated AEP is a key metric to assess the economic feasibility of a control strategy, and thus its eventual implementation. The proposed methodology provides an accurate tool, being based on high-fidelity simulations and exploiting the fast-convergence properties of gPC.

Acknowledgments

This work was partially supported by NSF I-UCRC WindSTAR (NSF Award IIP 1362033) and the members of the WindSTAR Industrial Advisory Board. TACC is acknowledged for providing computational time.

References

[1] Boersma S, Doekemeijer B M, Gebraad P M O, Fleming P A, Annoni J, Scholbrock A K, Frederik J A and van Wingerden J-W 2017 *Proc. of the 2017 American Control Conference*, pp. 1–18.
[2] Fleming P A, Gebraad P M O, Lee S, van Wingerden J-W, Johnson K, Churchfield M, Michalakes J, Spalart P, Moriarty P 2014 *Renew. Energy* **70**, 211–18.
[3] Jiménez Á, Crespo A, Migoya E 2010 *Wind Energy*, **13**, 559–72.
[4] Campagnolo F, Petrović V, Schreiber J, Nanos E M, Croce A, Bottasso C L 2016 *J. Phys.: Conf. Ser.*, **753**, 032006.
[5] Gebraad P M O, Teeuwisse F W, van Wingerden J W, Fleming P A, Ruben S D, Marden J R and Pao L Y 2016 *Wind Energy*, **19**, 95–114.
[6] Herbert-Acero J F, Probst O, Réthoré P-E, Larsen G C and Castillo-Villar K K 2014 *Energies*, **7**, 6930–7016.
[7] McKay M D, Beckman R J and Conover W J 1979 *Technometrics*, **21**, 239–45.
[8] Caflisch R 1998 *Acta Numer.*, **7**, 1–49.
[9] Adams B M, Bohnhoff W J, Dalbey K R, Eddy J P, Eldred M S, Gay D M, Haskell K, Hough P D and Swiler L P 2009 Tech. Rep. SAND2010-2183, Sandia National Laboratories.
[10] Xiu D and Karniadakis G E 2002 *SIAM J. Sci. Comput.*, **4**, 619–44.
[11] Xiu D and Karniadakis G E 2003 *J. Comp. Phys.*, **187**, 137–67.
[12] Sudret B 2008 *Reliab. Eng. Syst. Safe.*, **93**, 964–79.
[13] Ernst O G, Mugler A, Starkloff H-J and Ullmann E 2012 *ESAIM-Math. Model. Num.*, **46**, 317–39.
[14] Ciri U, Santoni C, Bernardoni F, Salvetti M V and Leonardi S 2019 *Proc. of the 2019 American Control Conference*, pp. 2849–54.
[15] Jensen N O 1983 Tech. Rep. Risø-M-2411, Risø National Laboratory.
[16] Katic I, Høistrup J and Jensen N O 1987 *Proc. of the European Wind Energy Conference*, pp. 407–10.
[17] Santoni C, Ciri U, Rotea M A and Leonardi S 2015 *Proc. of 2015 American Control Conference*, pp. 1715–20.
[18] Santoni C, Carrasquillo K, Arenas-Navarro I and Leonardi S 2017 *Wind Energy*, **20**, 1927–39.
[19] Smagorinsky J 1963 *Mon. Wea. Rev.*, **91**, 99-164.
[20] Ciri U, Petrolo G, Salvetti M V and Leonardi S 2017 *Energies*, **10**, 821.
[21] Orlandi P and Leonardi S 2006 *J. Turbul.*, **7**, N53.
[22] Leonardi S and Castro I P 2010 *J. Fluid Mech.*, 651, 519–39.
[23] Johnson K E, Pao L Y, Balas M J and Fingersh J L 2006 *IEEE Contr Syst Mag.*, **26** 70–81.
[24] Laks J H, Pao L Y and Wright A D 2009 *Proc. of the 2009 American Control Conference*, pp. 2096–2103.
[25] Rotea M A 2000 *Proc. of the 2000 American Control Conference*, pp. 433–7.

[26] Yang Z, Li Y and Seem J 2015 *J. Dyn. Syst.-T. ASME*, **137**, 121010.
[27] Ciri U, Rotea M A and Leonardi S 2017 *Renew. Energ.*, **113**, 1033–45.
[28] Ciri U, Rotea M A and Leonardi S 2018 *Wind Energy*, **21**, 1395–405.
[29] Jackson P S and Hunt J C 1975 *Q. J. Roy. Meteor. Soc.*, **101**, 929–55.
[30] Staffell I, Green R 2014 *Renew. Energ.*, 66, 775–86.
[31] Gebraad P M O and van Wingerden J-W 2015 *Wind Energy*, **18**, 429–47.
[32] Fleming P A, Ning A, Gebraad P M O and Dykes K 2016 *Wind Energy*, **19**, 329–44.
[33] Gebraad P M O, Thomas J J, Ning A, Fleming P and Dykes K 2017 *Wind Energy*, **20**, 97–107.
[34] Padrón A S, Thomas J, Stanley A P J, Alonso J J and Ning A 2019 *Wind Energ. Sci.*, **4**, 211–31.
[35] Kirchner-Bossi N and Porté-Agel F 2018 *Energies*, **11**, 3268